International Journal of Applied Glass Science 1–7 (2012)
DOI:10.1111/j.2041-1294.2012.00078.x

INTERNATIONAL JOURNAL OF
Applied Glass
SCIENCE

Raman Mapping of the Indentation-Induced Densification of a Soda-Lime-Silicate Glass

Assia Kassir-Bodon,* Thierry Deschamps, Christine Martinet, and Bernard Champagnon**

Laboratoire de Physico-Chimie des Matériaux Luminescents, UMR5620, CNRS, Université Lyon 1, Université de Lyon, F-69622, Villeurbanne Cedex, France

Jérémie Teisseire

UMR 125 CNRS/Saint-Gobain, Laboratoire Surface du verre et interfaces, 39 Quai Lucien Lefranc, F-93303, Aubervilliers, France

Guillaume Kermouche

LTDS UMR 5513 CNRS/ECL/ENISE, Université de Lyon, ENI Saint-Etienne, 58 rue Jean Parot 42023, Saint-Etienne Cedex 2, France

Micro-Raman spectroscopy was used to map the Vickers indentation-induced densification on a window glass (soda-lime silicate glass), from the correlation between Raman spectrum and density. Both top surface and cross-section of the residual imprints were investigated. It is shown that the sample preparation needed for the investigation of the in-depth densification does not alter the results. The maximum densification ratio measured is about 3.8%, which is 60% of the maximum densification measured after a high-pressure hydrostatic loading. Within the experimental errors, densification maps are self-similar for the two indentation loads used 10 N and 20 N. A comparison with finite element results based on a constitutive model developed for silica is discussed.

Introduction

The mechanical strength of the silicate glasses represents an important industrial issue. As it was recently underlined,[1,2] a lot of research effort has to be devoted to understand their mechanical behavior and improve their usable strength. Although primarily known as brittle materials at the macroscopic scale, glass was shown to undergo a plastic deformation under an indentation when its size does not exceed few tens of microns. The quantification and the mapping of the

**Member, The American Ceramic Society.
*assia.kassir-bodon@univ-lyon1.fr
© 2012 The American Ceramic Society and Wiley Periodicals, Inc

density of an indented glass at such a small scale is a challenge. Recent technical developments in the nano and micro-indentation field have led to significant advances. For example, Infra-Red,[3] micro-Raman spectroscopy,[4] and atomic force microscopy[5,6] were used to characterize the local deformation. The challenge was successfully taken up in the last years in the case of pure silica.[7–9] Perriot *et al.*[7] characterized the plastic deformation of amorphous silica after micro-indentation. Champagnon *et al.*[8] studied *in situ* elastic and plastic deformation of silica under a hydrostatic pressure by micro-Raman scattering. Vandembroucq *et al.*[9] discussed the elasto-plastic behavior of silica under pressure from a structural point of view**.** These results have led to the development of a constitutive model able to reproduce the indentation-induced densification in silica.[10] Extension of these experiments to the soda-lime silicate glasses, window or float glasses, is not straightforward.[11,12] The maximum densification ratio[11] in these glasses is much smaller than in silica (6.3%). A sharp indenter loading, like a Vickers, generates, beside densification, shear flows at the origin of shear bands. Luminescence of the samples due to a low percentage of trivalent chromium ions as impurities has been used to characterize the densification[13], but the broad luminescence of chromium is a severe drawback for Raman characterization using the usual laser excitations wavelengths. However, it was recently shown that *ex situ* Raman experiments can be performed on window glass densified in a diamond anvil cell.[14] The shift in the centroid of the main band is associated with the densification of the soda-lime glass. From this, a calibration curve was built and a top view mapping of the 10 or 20 N Vickers indentation was made.

In the present study, Vickers indentation experiments were performed with different loads. The permanent deformation is characterized by micro-Raman spectroscopy and a mapping of this deformation is done both from a top view and from a cross-section of the indentation imprint. The results are analyzed and discussed. They are then compared with results of finite element simulations based on the constitutive model previously developed for silica[10] and adapted to soda lime glasses.[13]

Experimental Procedure

Sample Preparation

The window glass (mainly components: 72% SiO_2, 15% Na_2O, 8% CaO, 4% MgO in mole%) is a standard float glass. On air face of the float glass plate (size $14 \times 8 \times 0.2$ cm^3) (Fig. 1a), two Vickers indentations of 10 N and two of 20 N were made. Vickers indents

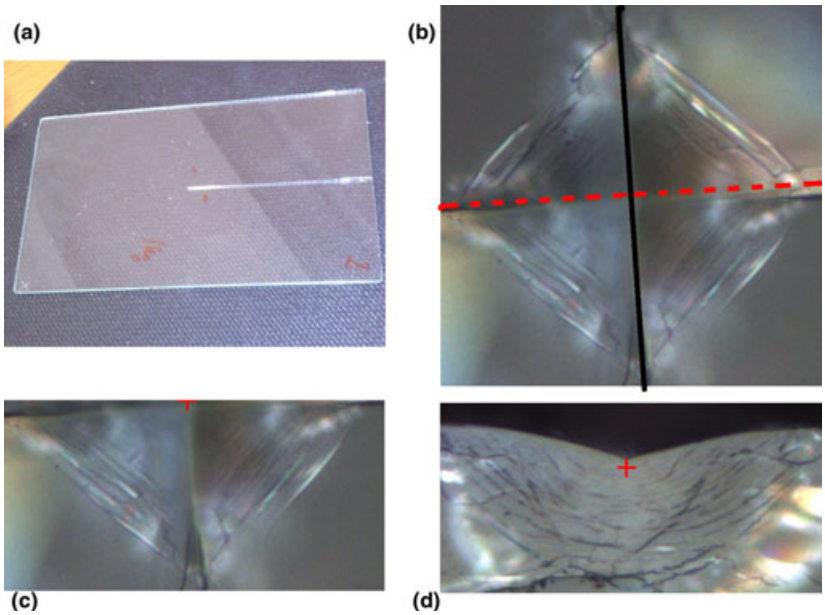

Fig. 1. Steps of side view realization for the window glass indented zone. (a) window glass plate precracked and indented, (b) 20 N indent top view image by optical microscopy, (c) cracked indent top view, (d) cracked indent side view.

were performed on a previously subcritically grown crack made with a double twist mechanism and outside of this crack (Fig. 1a). As shown on Fig. 1b, to minimize the mechanical perturbation due to the presence of the crack, we performed a symmetrical loading. The indenter was thus positioned so that one of the Vickers' pyramid diagonals is superimposed with the crack. The rupture of the indented sample on the crack is then completed by opening the crack. Two symmetrical sections of the indented area (Fig. 1c) are obtained. Figure 1d shows a cross-section of the sample. This procedure is detailed more accurately in Perriot *et al.*[7]

Experimental Setup

Raman spectra were obtained using a Raman Thermo-Fischer DXR spectrometer equipped with a microscopic attachment and a x, y, z stage. The laser YAG (Nd^{3+}) used for the 532 nm excitation delivers 10 mW on the sample. The signal is collected with a CCD in the range 50–1800 cm^{-1} with an accumulation time of 480 s, using a ULWD x 50 Olympus objective (numerical aperture 0.55, working distance 8 mm). The diameter of the laser spot and the z resolution are approximately 2 μm and 9 μm, respectively.[15]

Results

Experiment Results

Figure 2 shows two Raman spectra obtained on a window glass sample after a Vickers indentation with 20 N on his air face. One of the spectra (dotted line) was measured away from the indent; the other was measured in its center. Both spectra have several bands that are characteristic of the window glass structure.[14,16–18] In our work, we focused in the asymmetrical band in the domain 500–730 cm^{-1} which is more sensitive to densification. The position of its maximum located around 560 cm^{-1} is attributed to the symmetric vibration stretching mode of Si-O-Si Q_3 species (one nonbridging oxygen per SiO_2 tetraedron).[18] Its asymmetry is due to the presence of another component located at about 600 cm^{-1}. It is attributed to the vibration mode of Si-O-Si Q_2 species (two nonbridging oxygen tetraedron)[19] or to the D_2 silica band (three membered rings).[17] In addition, the figure shows that the Raman bands in the indent center are wider than in the nonindented part of the glass.

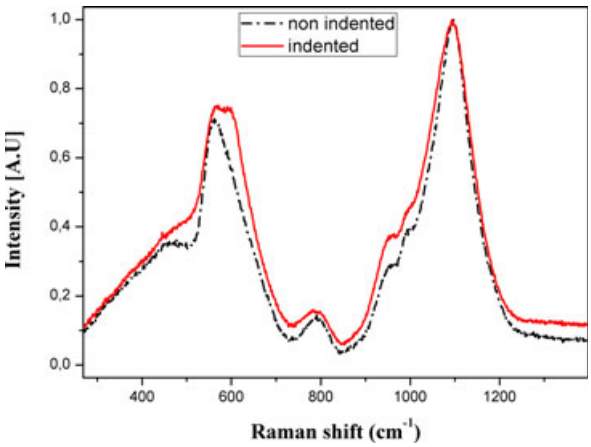

Fig. 2. Raman spectra of window glass on nonindented domain and at the center of an 20 N Vickers indent.

As shown in a previous paper[14] a Raman parameter $\Delta\sigma$ (cm^{-1}) can be used to characterize *ex-situ* the shift in the centroid of the band as a function of the maximum hydrostatic pressure reached. It was shown that $\Delta\sigma$ increases with maximum pressure reached between 6.9 and 16.2 GPa where the maximum densification ratio, $\Delta\rho/\rho_0$, is reached. From the study of Ji *et al.*[11], the maximum densification ratio of 6.3% was determined. In the frame of a linear approximation, it is then possible to build a calibration curve valid for maximum pressure reached between 6.9 and 16.2 GPa, which relates the densification ratio and the Raman parameter $\Delta\sigma$ (Fig. 3). From the slope of this curve, the following equation is obtained:

$$\Delta\rho/\rho_0 = 0,43\Delta\sigma \quad (1)$$

It makes it possible to directly connect the shift of the Raman band centroïd to the densification ratio $\Delta\rho/\rho_0$. $\Delta\sigma$ error due to the apparatus was fixed at ± 1 cm^{-1}. $\Delta\rho/\rho_0$ error was then calculated for each experimental point using Eq (1).

Figure 4 shows the top view mapping after 10 and 20 N indentations outside the precrack line region. On Fig. 4a is reported the shift of the centroïd of the band as function of the measured position from the indent center (position 0) along a parallel line to the diagonal of the indent (corresponding to the black line on Fig. 1b). The Fig. 4b depicts the same mapping with the $\Delta\sigma$ shift converted into densification ratio according to Eq (1) and the abscissa corresponding to the normalized distance to the center of the indent. The

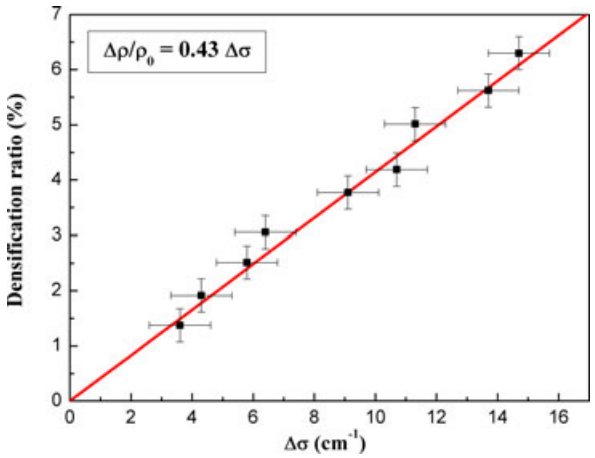

Fig. 3. Evolution of the densification ratio (%) versus the shift of the centroïd of the Raman band $\Delta\sigma$ (cm^{-1}).

normalized distance is obtained by dividing the position by the half width of the Vickers impression (30 μm for the 10 N load and 40 μm for the 20 N load).

On the Fig. 5 is plotted the top view mapping of the densification ratio as function of the normalized distance to the indent center for 20 N indents outside (black square) or on a precrack line (red circles).

From Raman measurements, it is possible to map the iso-density curves for the 20 N load in side view (Fig. 6a) and top view (Fig. 6b). These iso-density curves are compared with the microscopic optical observations showing the micro-cracking due to shear bands.

To test the cracks effect on the Raman bands, we performed an experiment on an isolated crack in a non-densified zone of the glass. The Raman signal is, in this case, similar to the Raman signal of the normal "non densified" glass.

Finite Element Analysis

In this section, the experimental maps are compared with results of a finite element analysis of the indentation test. These calculations are based on the constitutive model previously developed for silica[10] and adapted to window glass.[13] The yield limit is an elliptic criterion in the shear-pressure diagram. It is characterized by a limit under pure shear and a limit under pure hydrostatic pressure. The densification-induced hardening is modeled by taking into account an increase in

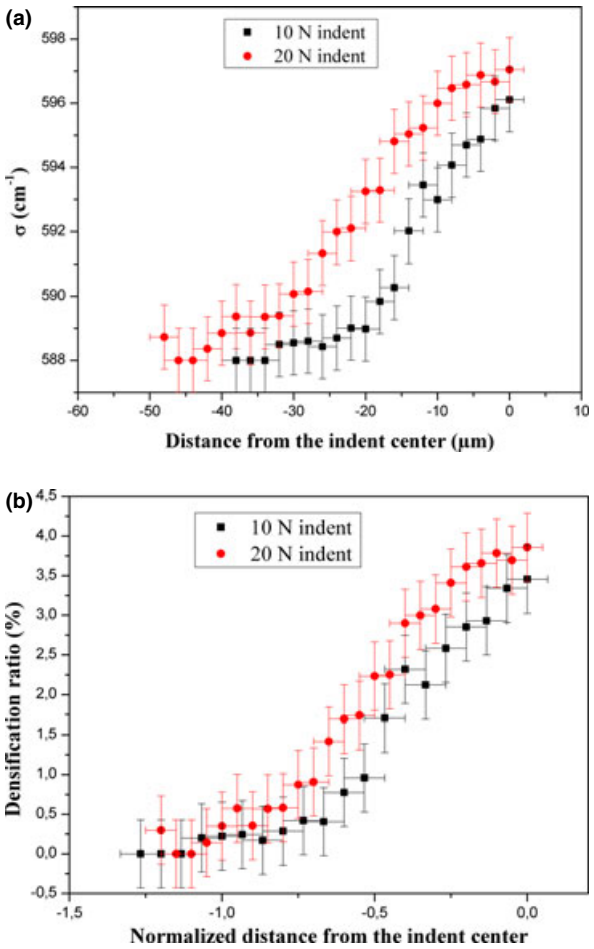

Fig. 4. (a) Top view mapping of the Raman shift of the centroid of the band outside a precrack domain for 10 N and 20 N Vickers loads. (b) Top view mapping of the densification ratio as function as the normalized distance from the indent center outside a precrack domain for 10 N and 20 N Vickers loads.

hydrostatic limit with the permanent densification of the material measured.[11] The shear limit does not depend on the permanent densification. Calculations have been performed with the Finite Element Software Systus[20] using 3D elements and using a large displacement/large strain option (updated Lagrangian formulation, logarithmic strain). The boundary and loading conditions are similar to those proposed by Giannakopoulos *et al.*[21] More details on this model can be found in the studies of the authors.[10,13]

Two different densification maps are plotted in Fig. 7. The first one is the densification computed taking into account both elastic and plastic deformations

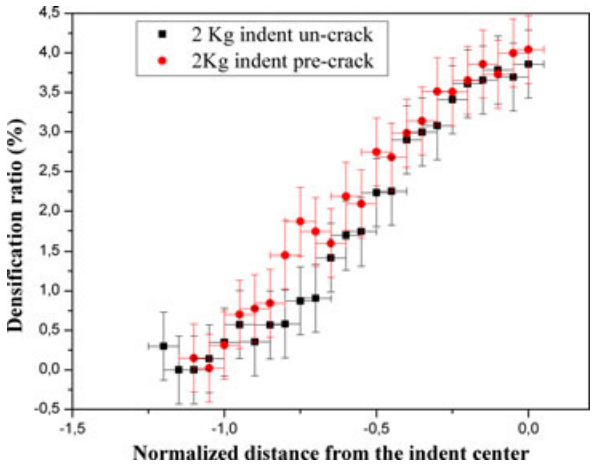

Fig. 5. Top view mapping of the densification ratio as function of the normalized distance from the indent center for 20 N indent outside (black square) or on a precrack line (red circles).

(Fig. 7a). As shown in Fig. 1b**,** there are several cracks in the contact region. It can thus be assumed that the elastic energy stored is released during the propagation of these cracks. Consequently, we have also computed the densification by taking into account only the plastic strain (Fig. 7b). In this case, the densification is two times lower. It points out that contrary to silica, the magnitude of the bulk plastic deformation and the bulk elastic deformation are of the same order of size. A quite good agreement with the densification computed from the plastic strain only can be observed.

Discussion

Results in Fig. 2 show that the 500–730 cm^{-1} band is modified during the Vickers indentation. In particular, the relative intensity of the Raman bands suggests a decrease in Q_3 species at the expense of Q_2 species.[14] These structural changes are reflected at the macroscopic scale by a permanent densification of the window glass. Observe that the maximum ratio of densification of the window glass (6.3%) is much lower than that of silica (20%). Despite the width of the Raman band, it is possible to establish a calibration curve allowing the direct determination of the densification ratio from the Raman shift of the centroïd of the band.

On Fig. 4b, it is then shown that the maximum densification ratio at the center of the indent is approximately equal within the experimental errors for the 10 N (3.6%) and for the 20 N (3.8%) loads. A part of this experimental error is due to the z resolution of the X50 objective (9 µm).It means that the Raman analysis is performed with an integration of the Raman signal over 9 µm for both 10N and 20 N loads,

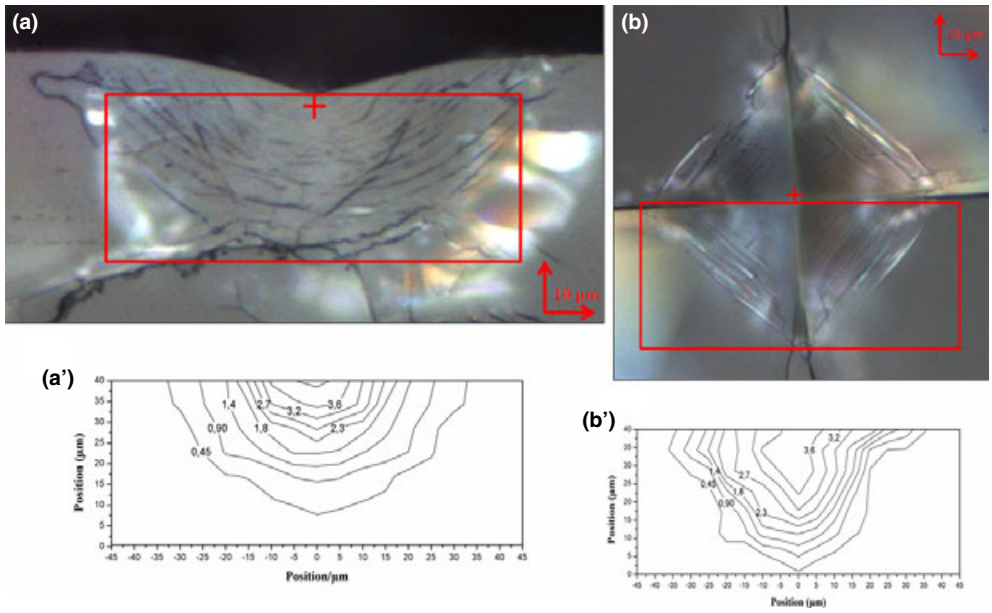

Fig. 6. Optical microscope and Raman mapping of the iso-density curves for a 20 N Vickers load in side view (a,a′) and top view (b,b′).

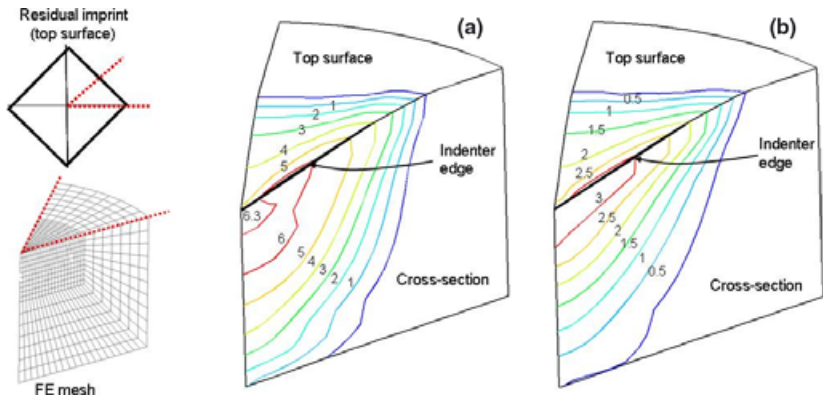

Fig. 7. Densification maps calculated from the finite element simulations, (a) densification computed taking into account the total volumic strain (elastic + plastic), (b) densification computed in taking into account only the plastic volumic strain (we consider here that the elastic energy is released by crack initiations and propagations).

whereas the half width of the Vickers indent are respectively 30 μm and 40 μm. The densification determined in these conditions is then averaged over a density gradient larger for the 10 N load than for the 20 N load. This leads to a lower apparent density at the center of the indent. The normalization of the abscissa by the width of the indent shows further that both curves coincide within the experimental errors. This result is in agreement with the well-known self-similarity of sharp indentation.[22] This principle states that if two indentations are made by the same geometric shapes, then, whatever their size, strain and stress fields around indentation will be geometrically similar.[10] Here, the consequence of this self-similarity is that the indentation-induced cracks do not affect the densification process for the range of load used (10 N and 20 N). It is probably because the loads used are much higher than the limit load under which no micro-cracks are created, and thus there is enough micro-cracks in the region of the contact to consider the material as macroscopically homogeneous. This point is of primary importance for the development of a constitutive model.

The overlay of the curves (Fig. 5) for indentations outside or on a precrack line shows that this line does not influence the indentation. The results obtained in this way for the side-view measurements are representative of the indentation without any modification due to the precracking of the sample. It points out that the sample preparation does not alter the result. Hence, the side-view mapping is more easily compared with the Finite Element simulations.

In agreement with this observation, the iso-density mapping has different aspects. The side view corresponds to a "bowl" shape aspect, whereas the top view corresponds more to a "star" aspect. The bowl shape on the cross-section is also observed with the finite element analysis as well as a good agreement in terms of densification gradient. However, the density variation over the top surface is badly reproduced, which points out that the constitutive model is not really appropriated. It is worth observing the correlation between the iso-density curves and the distribution of cracks (shear bands) for both loads. On the one hand, it could suggest that the densification of the window glass is strongly affected by the shear flow and consequently, the development of a constitutive model for the window glass should take into account this feature. On the other hand, it may also be considered as a weakness of the above results that the occurrence of these cracks can modify the Raman bands, and thus the distribution could be considered as nonrepresentative of what happened at a lower scale. According to some authors, the minimum indentation load inducing cracks is about 100 mN for window glass. However, the size of the indented zone is then too small to allow a precise mapping of the density (lateral resolution of the Raman analysis cannot be set below 1 μm with a normal ×100 objective). The validity of our approach is checked by the fact that the cracks do not modify significantly the Raman spectra. One complementary question addressed by the finite element analysis is the quantitative analysis of the maximum densification. From Fig. 7, the densification at the center of the indent is only the half of the maximum densification of the window glass if we consider that the elastic stresses are released by the microcracks. This is in agreement with our experiments where only 60% of the maximum of the densification is mea-

sured at the indent center. Here again, the mapping of low load indents could help clarify this point. This will be discussed in future investigations.

Conclusion

The Raman micro-spectroscopy is an efficient tool to map the local density distribution on Vickers imprints in a window glass. It is shown that the densification map was self-similar for the two loads used, and that the densification distribution was not altered by the sample preparation: the validity of side-view measurements on indents performed on a precrack line was demonstrated. Hence, the maps measured may be considered as representative of the plastic flow of the window glass under Vickers indentation. Due to the limitation of the spatial resolution of the Raman excitation, such mapping is, however, significant only on indents performed on large loads, which are unfortunately responsible of shear bands and micro-cracks. It was observed that these cracks develop along the iso-density curves. To check the role of the interaction between the densification process and the shear bands, measurements on 100 mN and 500 mN indents are in progress. The comparison with finite element results based on a constitutive model developed for silica reveals a good agreement over the cross-section, but this agreement is less satisfying over the top surface. Let us note here that it has been assumed that the bulk elastic deformation has been released by the micro-cracks and consequently, the densification has been computed taking only into account the bulk plastic deformation. A better agreement over the top surface is expected from the development of a specific constitutive model to reproduce the plastic flow of the window glass, and especially shear bands failure phenomena. The shape of the densification area and the quantitative gradient determined from these experiments is a rich set of data to develop such a new constitutive model.

Acknowledgments

The authors thank E. Barthel and R. Lacroix (SVI Saint-Gobain) for fruitful discussions and the indented glass preparation. This work was supported by the 'Region Rhône-Alpes' program MACODEV and extensively used the "CECOMO" facility of the "Institut de Chimie de Lyon."

References

1. C. R. Kurkjian, P. K. Gupta, and R. K. Brow, "The Strength of Silicate Glasses: What do We Know, What do we Need to Know," *Int. J. Appl. Glass Sci.*, 1 [1] 27–37 (2010).
2. C. R. Kurkjian, "Towards a Glass with Higher Usable Strength: The Need to Develop Collaborations," *Int. J. Appl. Glass Sci.*, 1 [3] 216–220 (2010).
3. A. Koike and M. Tomozawa, "IR Investigation of Density Changes of Silica Glass and Soda-Lime Silicate Glass Caused by Microhardness Indentation," *J. Non-Cryst. Solids*, 353 2318–2327 (2007).
4. A. Kailer, K. G. Nickel, and Y. G. Gogotsi, "Raman Microspectroscopy of Nanocrystalline and Amorphous Phases in Hardness Indentations," *J. Raman Spectrosc.*, 30 939–946 (1999).
5. S. Yoshida, J.-C. Sangleboeuf, and T. Rouxel, "Quantitative Evaluation of Indentation-Induced Densification in Glass," *J. Mater. Res.*, 20 [12] 3404–3412 (2005).
6. E. C. Ziemath and P. S. P. Herrmann, "Densification and Residual Stresses Induced in Glass Surfaces by Vickers Indentations," *J. Non-Cryst. Solids*, 273 19–24 (2000).
7. A. Perriot *et al.*"Raman Microspectroscopic Characterization of Amorphous Silica Plastic Behavior," *J. Am. Ceram. Soc.*., 89 [2] 596–601 (2006).
8. B. Champagnon *et al.*"High Pressure Elastic and Plastic Deformation of Silica: In Situ Diamond Anvil Cell Raman Experiments," *J. Non-Cryst. Solids*, 354 569–573 (2008).
9. D. Vandembroucq *et al.*"Density Hardening Plasticity and Mechanical Ageing of Silica under Pressure: a Raman Spectroscopic Study," *J. Phys.: Condens. Matter*, 20 485221 (2008).
10. G. Kermouche, E. Barthel, D. Vandembroucq, and Ph. Dubujet, "Mechanical Modeling of Indentation-Induced Densification in Amorphous Silica," *Acta Mater.*, 56, 3222–3228 (2008).
11. H. Ji, V. Keryvin, T. Rouxel, and T. Hammouda, "Densification of Window Glass under Very High Pressure and its Relevance to Vickers Indentation," *Scripta Mater.*, 55 1159–1162 (2006).
12. S. Yoshida, J.-C. Sangleboeuf, and T. Rouxel, "Indentation-Induced Densification of Soda-Lime Silicate Glass," *Int. J. Mat. Res.*, 98, 360–364 (2007).
13. A. Perriot, E. Barthel, G. Kermouche, G. Querel, and D. Vandembroucq, "On the Plastic Deformation of Soda-Lime Glass-a Cr(3+) Luminescence Study of Densification," *Phil. Mag.*., 91 1245–1255 (2011).
14. T. Deschamps, C. Martinet, J.-L. Bruneel, and B. Champagnon, "Soda-Lime Silicate Glass under Hydrostatic Pressure and Indentation: a Micro-Raman Study," *J. Phys.: Condens. Matter*, 23, 035402 (2011).
15. Dilor Confocal Laser Application note (1992).
16. D. W. Matson, S. K. Sharma, and J. A. Philpotts, "The Structure of High-Silica Alkali-Silicate Glasses. A Raman Spectroscopic Investigation," *J. Non-Cryst. Solids*, 58 323–352 (1983).
17. J. E. Dickinson Jr, C. Scarfe, and P. McMillan, "Physical Properties and Structure of $K_2Si_4O_9$ Melt Quenched from Pressures up to 2.4 GPa," *J. Geophys. Res.*., 95 15675–15681 (1990).
18. P. McMillan, "Structural Studies of Silicate Glasses and Melts-Applications and Limitations of Raman Spectroscopy," *Am. Mineral.*., 69 622–644 (1984).
19. X. Y. Xue, J. F. Stebbins, M. Kanazaki, P. F. McMillan, and B. Poe, "Pressure-Induced Silicon Coordination and Tetrahedral Structural Changes in Alkali Oxide-Silica Melts up to 12 GPa: NMR, Raman, and Infrared Spectroscopy," *Am. Miner.*, 76 8–26 (1991).
20. Systus/Sysweld. *Users's manual.* ESI Group, Paris, 2011.
21. A. E. Giannakopoulos, P. L. Larsson, and R. Vestergaard, "Analysis of Vickers Indentation," *Int. J. Solids Struct.*., 31 2679–2708 (1994).
22. Y.-T. Cheng, and C.-M. Cheng, "Scaling, Dimensional analysis, and Indentation Measurements," *Mat. Sci. Eng.*, 44, 91–149 (2004).